JOURNAL OF MATERIALS SCIENCE **36** (2001) 4995 – 5005

Characterization of structural alumina ceramics used in ballistic armour and wear applications

ADEBAYO Y. BADMOS, DOUGLAS G. IVEY
Department of Chemical and Materials Engineering, University of Alberta, Edmonton, Alberta, Canada, T6G 2G6

Structural alumina ceramics used in ballistic armour and wear applications with varying alumina contents and manufactured using both slip casting and dry pressing techniques, have been investigated and characterized in terms of their hardness, elastic modulus, fracture toughness, and microstructural characteristics. For a given alumina content, fracture toughness decreases with increasing hardness. Dry pressed samples show slightly higher hardness, and lower fracture toughness for the same alumina content. The hardness, elastic modulus and fracture toughness are higher for the 98% alumina samples while the differences between the lower alumina samples (95 and 91%) are negligible. The grain sizes are bimodal with the majority ≤ 3 μm and the size range narrows with decreasing alumina content. The microstructures are composed of a matrix phase, corundum (α-Al_2O_3), grain boundary phases consisting of a glassy phase with varying Al_2O_3, SiO_2, and CaO contents, a crystalline phase, triclinic anorthite ($CaAl_2Si_2O_8$), and an additional phase, spinel ($MgAl_2O_4$), in the lower alumina samples. The proportion of the boundary phase increases with decreasing alumina content and no effect of fabrication method is observed.

1. Introduction

Structural alumina ceramics for ballistic armour and wear applications are manufactured using either a slip casting or a dry pressing technique. Slip casting is an effective process for producing quantities of complex parts or low volumes of simple parts when tooling cost makes it prohibitive by alternative means. It is, however, a very slow and labour intensive process and the cost of parts produced using the technique is higher compared to more automated processes such as dry pressing. Moreover, a high precompaction and sintering without a liquid phase are the main characteristics of the production process of high alumina ceramics. Slip casting, in general use in the manufacture of almost all other ceramic materials, is normally not applied to high alumina ceramics because of insufficient precompaction [1]. Other methods such as dry pressing, hydrostatic molding, extrusion, injecting moulding, and hot pressing have proven to be practical and successful in compacting alumina powders.

Dry pressing is the most common and most economical process for the fabrication of high alumina ceramics, although, it is restricted to parts with simple shapes and to wall thickness greater than 1 mm [1]. Generally, dry pressing is the most fundamental method used in the manufacturing of flat ceramic tiles for both the wear and armour markets.

However, in order to perform the dry pressing operation successfully a firm understanding of both the mechanics of the pressing operation and the properties of the powder being pressed is required. The production of the dry pressed materials with desirable properties, at least comparable to slip cast ceramics, is a challenge with a number of technical barriers to overcome. For example, there will be notable differences in the properties of the dry pressed material compared to the slip cast ceramic, given the difference in the processing routes of the powders. In the slip casting process, the powders are very finely dispersed and are deposited in the mould cavity slowly and uniformly producing a very homogeneous structure. In dry pressing, the same finely dispersed powder is first spray dried into agglomerated pellets of the powder and then crushed into a solid mass under pressure. Distinct grain boundaries and pores exist between the crushed pellets, which can persist through to the fired body [2]. Moreover, the shrinkage rate depends on the amount of precompaction [3]; the lower the precompaction, the higher the shrinkage rate and non-uniform compaction within the same body leads to variable shrinkage and consequently to warping, cracking and development of internal stresses. Therefore, the performance of pressed ceramics will depend on how well the spray-dried powder can be compacted and sintered to full density.

Generally, performance characteristics of structural alumina ceramics depend on the details of their microstructures, which are determined largely by the purity of the starting powder, composition of the additives, fabrication technique and the sintering conditions. The present work investigates samples of structural alumina ceramics manufactured using both slip casting and dry pressing fabrication techniques and with varying

TABLE I Alumina ceramic samples investigated

Sample	Alumina content (wt%)	Processing method
SC98-1	98	Slip casting
SC98-2	98	Slip casting (optimized)
DP98-1	98	Dry pressing
DP98-2	98	Dry pressing (lower viscosity)
SC95-1	95	Slip casting
SC95-2	95	Slip casting (different source)
SC91-1	91	Slip casting
SC91-2	91	Slip casting (different source)
DP91-1	91	Dry pressing

alumina contents and other fabrication parameters. The various samples were characterized in terms of their hardness, elastic modulus, fracture toughness and microstructural characteristics.

2. Experimental techniques

2.1. Materials

The Ceramic Protection Corporation (CPC), Calgary supplied the alumina products investigated, and the various samples are described in terms of Al_2O_3 content and processing method in Table I. The ceramic samples vary either in terms of alumina content, density, manufacturing process or grade of raw materials used. They are in three sets containing 98%, 95% and 91% alumina and are accordingly designated with a prefix indicating whether the manufacturing process was by slip casting (SC) or by dry pressing (DP) and a terminal number to distinguish between variants of the same kind. The additives consist of SiO_2, CaO, and MgO and are in different proportions for the various alumina contents.

The SC98-1 and SC98-2 samples were both manufactured by the slip casting method, but SC98-2 was produced using an improved proprietary process, i.e., an optimized dispersant content, a modern kiln and an optimized kiln firing profile. The difference between the dry-pressed, 98%, DP98-1 and DP98-2 samples is that they were produced using press-powders manufactured from slips with different viscosities and specific gravities (lower for DP98-2) and different spray drying parameters. The 95% samples, SC95-1 and SC95-2, and 91% samples, SC91-1 and SC91-2, are slip cast products, but manufactured with raw materials from different sources. DP91-1 is a 91% alumina sample produced using the dry pressing technique.

2.2. Mechanical properties

2.2.1. Hardness and fracture toughness

An indentation technique [4] was used for the determination of the fracture toughness and hardness of the ceramic materials. The indentation technique is a simple, inexpensive alternative to the ASTM E399-90 standard procedure for measuring fracture toughness. The correlation between values obtained from both toughness values has been shown to be reasonably good for ceramic materials [5]. A routine hardness testing facility was used to make Vickers indentations on the optically prepared sample surfaces. The indented surfaces were then examined by optical microscopy, in reflected polarized light. The characteristic dimensions of the plastic impression and the indentation-induced cracks were measured as averages over the two orthogonal radial directions.

The fracture toughness, K_c, is defined by [4]:

$$K_c = 0.02473 \cdot E^{1/2} \cdot a \cdot \frac{P^{1/2}}{c^{3/2}} \quad (1)$$

where $2c$ is the radial crack length, P the applied load, E the Young's Modulus and $2a$ the diagonal of the indentation impression.

The Vicker's hardness values, H_v, were obtained from a conversion table which is the same as the expression

$$H_v = 1.8544 \frac{P}{d^2} \quad (2)$$

where $d = 2a$ in mm and P is in kg.

The samples were found to satisfy all the conditions required for the technique to be applicable, as explained in detail by Ostojic and McPherson [4]. At the different loads, 5–10 indentations were made on each sample. Subsequent calculations were made using the mean values of the impression diagonals and the radial crack lengths. Standard deviations for the measured quantities were determined and used in determining the errors in the calculated fracture toughness and hardness.

2.2.2. Elastic modulus

A Knoop indentation testing technique [6, 7] was used to measure the elastic modulus of the ceramic samples. This method is based on the measurement of the elastic recovery of the surface impression of the indentation diagonals (a and b) made by Knoop indenter. The elastic recovery is independent of load and is correlated with the hardness (H) to elastic modulus (E) ratio as follows:

$$\frac{b'}{a'} = \frac{b}{a} - \alpha \frac{H}{E} \quad (3)$$

where a' and b' are the dimensions of the Knoop diagonals after elastic recovery, and α is a constant. The value of α determined by curve-fitting the experimental data to Equation 4 is 0.45 [6] and the values of a, b, a' and b' are obtained from the Knoop indentations. The elastic recovery ($b'/a' - b/a$) was evaluated with a known value of a/b (7.11) for the Knoop indenter geometry and H was obtained from the Vicker's hardness measurements to estimate E. As indicated by Marshall *et al.* [6], the relative error in the estimation of H/E is $<10\%$ for most brittle materials.

2.3. Microstructural characterisation

Microstructural analysis was carried out using a combination of scanning electron microscopy (SEM), transmission electron microscopy (TEM) and X-ray diffractometry (XRD). Microchemical analysis was performed using energy dispersive X-ray (EDX) spectroscopy in the SEM and TEM.

Materials for microstructural characterization using SEM were prepared as for normal metallographic studies and thermally etched. Thermal etching of the samples was accomplished by heating the samples in air at 1400°C for one hour and the preferential volatilization of material from the grain boundaries provides the etching. A Hitachi H2700 SEM equipped with an energy dispersive X-ray (EDX) detector was used for the microtructural and composition analysis. Analysis of the grain structure and apparent porosity were conducted using linear and area intercept methods respectively on the SEM images collected at various locations from each of the samples. Specimens for TEM were prepared using the standard procedures for ceramic materials. Disks, 3 mm in diameter and about 250 μm thickness, were mechanically dimpled, sputtered in an ion mill to perforation and evaporation-coated with a thin layer of carbon. The specimens were observed in a JEOL 2010 TEM, equipped with an ultra thin window (UTW) energy dispersive X-ray (EDX) detector. Phase identification was achieved using a combination of electron diffraction and EDX information. X-ray diffractometry analysis of powder samples was conducted using a Rigaku X-ray diffractometer system, DMAXB. The XRD patterns were processed using JADE, XRD pattern-processing software equipped with a Search/Match module for phase identification using the ICDD (International Centre for Diffraction Data) PDF (Powder Diffraction File) and/ or user-created databases.

3. Results and discussion

3.1. Mechanical properties

Table II shows the hardness, H_v, Young's Modulus, E, and fracture toughness, K_c, determined for the various ceramic samples with an indentation load of 100 N. Also included in Table II is the ratio H/K_c, (H is H_v expressed in GPa) proposed by Lawn and Marshall [8] as a measure of the index of brittleness. However, the parameter, H/K_c does not appear to provide any additional insight into the behaviour of these materials and will not be mentioned in the subsequent discussion.

Generally, hardness, elastic modulus, and fracture toughness are higher for the 98% alumina samples, while the differences between the 95% and 91% alumina samples are not significant. The dry pressed samples show slightly higher hardness but lower fracture toughness than the slip cast samples of the same composition. This is shown by the results for DP98-1 and DP98-2 compared with SC98-1 and SC98-2 and also DP91-1 compared with SC91-1 and SC91-2.

TABLE II Hardness, Young's modulus, fracture toughness, and index of brittleness for an indentation load of 100 N

Sample	H_v (Kg/mm^2)	H (GPa)	E (GPa)	K_c (MPa $\cdot$ m$^{1/2}$)	H/K_c (μm$^{-1/2}$)
SC98-1	1288 ± 37	12.6	299 ± 30	3.09 ± 0.2	4.0
SC98-2	1354 ± 34	13.3	325 ± 15	2.98 ± 0.1	4.5
DP98-1	1402 ± 75	13.8	299 ± 60	2.91 ± 0.4	4.7
DP98-2	1478 ± 44	14.5	289 ± 76	2.77 ± 0.1	5.2
SC95-1	1097 ± 58	10.8	226 ± 50	2.33 ± 0.3	4.6
SC95-2	1187 ± 66	11.6	251 ± 38	2.30 ± 0.2	5.0
SC91-1	1132 ± 35	11.1	259 ± 34	2.51 ± 0.1	4.4
SC91-2	1150 ± 16	11.3	229 ± 18	2.37 ± 0.2	4.8
DP91-1	1168 ± 34	11.5	241 ± 29	2.37 ± 0.2	4.9

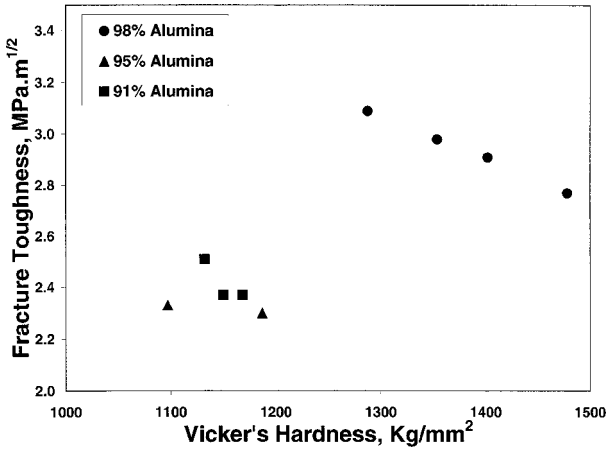

Figure 1 Variation of fracture toughness with hardness for ceramic products with different alumina compositions.

Fig. 1 shows the variation of the fracture toughness, K_c, with hardness, H_v, for samples with different alumina compositions. For the same alumina content, fracture toughness is shown to decrease with increasing hardness. Generally, the dry pressed samples show higher hardness and lower fracture toughness values than the slip cast samples. The low fracture toughness may be due to the less homogeneous structure of a dry pressed ceramic compared to the slip cast products. In slip casting, the ceramic powders are finely dispersed in the mould cavity slowly and uniformly producing a very homogeneous structure, whereas, in dry pressing, the same finely dispersed powder is first spray dried into agglomerated pellets and then crushed into a solid mass. Distinct boundaries and pores exist between the crushed pellets, which can persist through to the fired body [2].

3.2. Microstructural characteristics

Typical SEM images of the slip cast and dry pressed thermally etched 98% alumina samples are shown in Fig. 2 and those of the 95% and 91% alumina samples are shown in Fig. 3. Table III presents the average grain sizes, approximate size ranges, approximate size distribution, and percent apparent porosities determined for the different ceramic samples.

The differences in the microstructures of the two slip cast 98% alumina samples (Fig. 2a and b) show the effect of processing parameters on the microstructures. The manufacturing of SC98-2 (Fig. 2a) was accomplished using an optimized process (i.e., dispersant content, kiln firing profile and a more modern firing kiln, among other parameters) compared with SC98-1. As shown in Table III, SC98-2 shows a finer and more homogeneous grain structure than SC98-1. This is consistent with the hardness values of the samples (Table II). The finer and more homogeneous grain structure in SC98-2 has produced a higher hardness. Consistent with the general pattern, the fracture

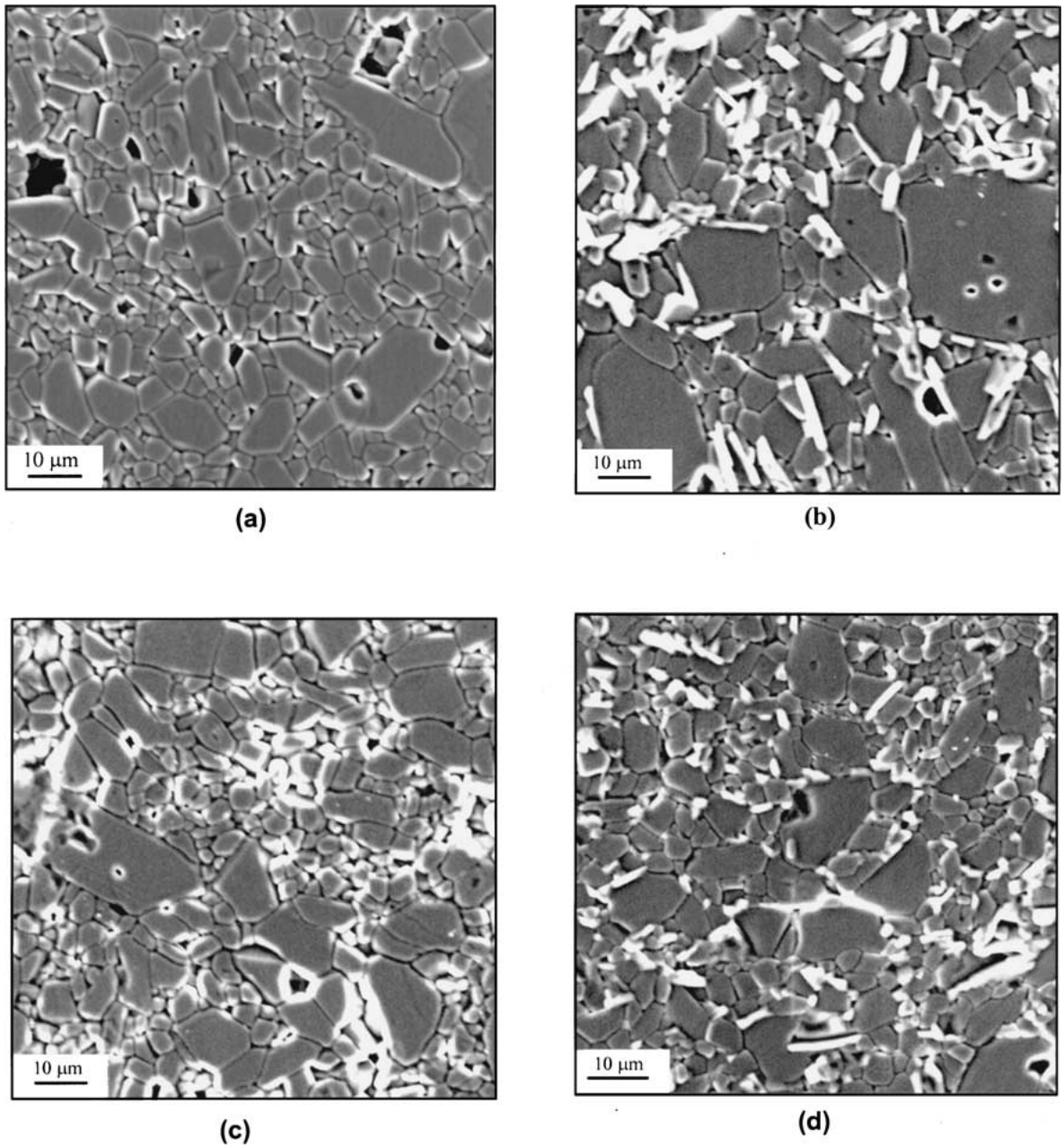

Figure 2 SEM images of the 98% alumina samples. Slip cast—(a) SC98-2 and (b) SC98-1; Dry pressed—(c) DP98-1 and (d) DP98-2.

TABLE III Average grain sizes and apparent porosities of the various ceramic samples

Sample	Average grain size (μm)	Approx. size range (μm)	Approx. size distribution		Apparent porosity (%)
			$\leq$3.0	>3.0 μm	
SC98-1	3.89 ± 0.21	0.5–16.0	69%	31%	09 ± 1.2
SC98-2	3.25 ± 0.23	0.8–13.0	91%	9%	16 ± 1.8
DP98-1	3.17 ± 0.22	0.3–14.0	87%	13%	11 ± 2.1
DP98-2	3.07 ± 0.24	0.3–10.0	89%	11%	08 ± 3.1
SC95-1	3.62 ± 0.38	0.5–11.0	80%	20%	21 ± 7.0
SC95-2	3.89 ± 0.56	1.0–11.0	76%	24%	30 ± 5.2
SC91-1	3.92 ± 0.46	0.5–6.3	83%	17%	29 ± 4.3
SC91-1	3.33 ± 0.15	0.5–5.8	90%	10%	31 ± 3.4
DP91-1	3.33 ± 0.24	0.8–5.8	89%	13%	39 ± 6.1

toughness of SC98-2 is correspondingly lower than that of SC98-1.

There is no obvious difference between the grain structure of the optimized slip cast sample SC98-2 (Fig. 2a) and the dry pressed 98% samples DP98-1 and DP98-2 (Fig. 2c and d). However, the grain structure of DP98-2 is a bit finer and the grain size is more homogeneous than for DP98-1 (Table III). Although, they are both dry pressed samples, the characteristics of the slips from which the powders were prepared and the spray drying parameters were different. Most importantly, the viscosity and specific gravity of the slip were lower for the DP98-2 than they were for the DP98-1.

The finer grain size and more homogeneous structure in SC98-2 compared with SC98-1 and in DP98-2 compared with DP98-1 does not produce a correspondingly better hardness and fracture toughness. Within the limit of accuracy of the indentation technique used, the differences in the fracture toughness of all the 98% alumina samples are negligible. Moreover, a comparison of the published data on the influence of grain size on fracture mechanics parameters of polycrystalline ceramics does not always reveal clear trends.

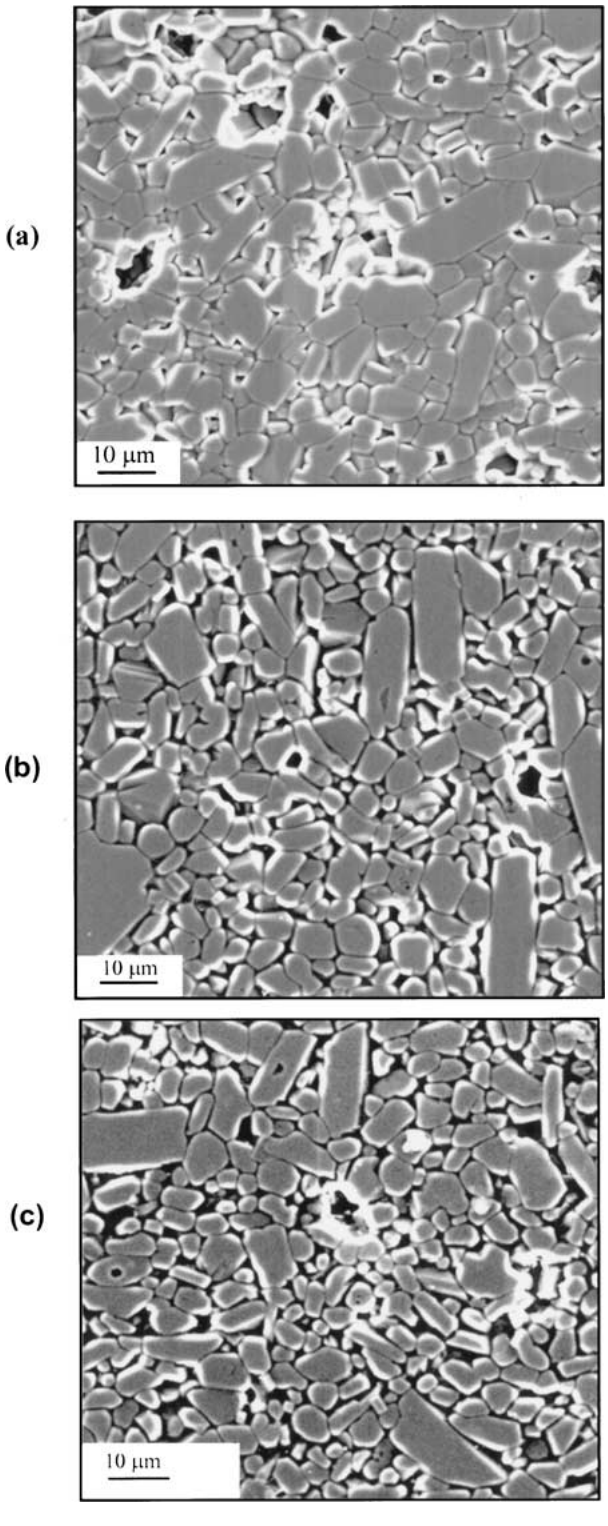

Figure 3 SEM images of (a) SC95-1 (slip cast), (b) SC91-1 (slip cast) and (c) DP91-1 (dry pressed).

Some variations will be due to differences in the microstructural characteristics that influence toughness, and the difficulty in studying them independently [9]. Toughness values have been reported, which either decrease [10] or increase [11, 12] with increasing grain size. In a review of intergranular fracture of polycrystalline ceramics, Pratt [13] has suggested that the disagreement in the dependence of toughness on grain size may stem partly from the use of different testing techniques. Dalgleish *et al*. [9] investigated the influence of grain size on the fracture toughness of polycrystalline alumina using the single edge-notched beam (SENB), the double-cantilever beam (DCB), and the double torsion (DT) techniques. The toughness values from SENB and DCB tests were reported [9] to have shown an overall decrease with increasing grain size, whereas the values from double torsion tests showed little change. Steinbrech *et al*. [14] reported that finer grained alumina ceramics showed a higher crack resistance force at the initiation of cracking but lost that beneficial effect during further propagation.

As shown in Fig. 3, there is no difference between the grain structures of the slip cast and dry pressed 91% samples. The grain structure of the 95% alumina sample appears coarser than that of the 91% samples, but finer than the 98% samples in Fig. 2. However, as shown in Table III, the differences in the measured average grain sizes of the 95% and 91% samples are negligible. The wide size ranges for the 95% samples, indicating a less homogeneous structure, explains this. The SC95-1 and SC95-2 samples were produced using slip casting but the raw materials were from different sources. As shown in Table III, within the error limits, their grain sizes are similar but as indicated by the smaller size range, SC95-2 shows a more homogeneous grain structure and this likely explains its higher hardness and lower fracture toughness (Table II). SC91-1 and SC91-2 were both produced by slip casting but the raw materials were from different sources. SC91-2 shows a finer and more homogeneous grain structure (Table II) and its hardness is slightly higher and fracture toughness lower than SC91-1. The dry pressed sample, DP91-1, has a similar grain size to SC91-2 but the grain structure is a bit more homogeneous (Table III) and this explains the slightly higher hardness but similar fracture toughness values (Table II).

Generally, the microstructures of the samples are characterized by mixed grain sizes with some differences in the range and distribution. The grain sizes in all the samples are bimodal with some grains that are small and some that are quite large. Except for SC98-1, the populations of small grains are very high in the 98% alumina samples and are only interspersed by larger grains. The grain size is most homogeneous in the 91% alumina samples.

The average grain sizes of the dry pressed samples are slightly smaller than those of the slip cast samples of the same composition and this explains their higher hardness values. Approximate size ranges are shown to reduce with decreasing alumina content indicating increasing grain size uniformity with decreasing alumina content. The approximate size distributions show that the majority of grains in all the samples are very fine ($\approx$3.0 μm). However, the proportion of large grains is shown to be quite substantial in SC98-1, which is obvious from the microstructure (Fig. 2b). Generally, apparent porosity appears to increase with decreasing alumina content. However, these high values may be due to grain pullout. Grain pullout during sample polishing is a well-known problem with high alumina ceramics. A combination of the residual stresses from the second phases and the stresses created during grinding has been

reported to enhance pullout of alumina grains [15]. A higher proportion of porosity/secondary phase would explain the lower hardness and fracture toughness in the lower alumina samples. Porosity in ceramics acts much like an internal flaw and lowers fracture toughness [16]. A glassy secondary phase, shown later to be more pronounced in the low alumina samples, is the weakest link in the chain of load-bearing microstructural features within the sintered body [17].

The TEM microstructures show the proportion of the secondary phase to increase with decreasing alumina content (Fig. 4). In the 98% alumina samples, the secondary phase is mainly found at the triple-points of the alumina matrix grains (Fig. 4a), whereas in the 91% samples, in some areas, the alumina grains are totally embedded in the secondary phase (Fig. 4c). Although, the boundary phase appears to be discrete, it has been reported to be continuous and that it wets most of the boundaries except low angle boundaries and special boundaries such as basal and rhombohedral twins [18–20]. As mentioned earlier, the Al_2O_3 grain size distribution is bimodal, consisting of grains less than 3 μm in size (above 80%) and those significantly greater than 3 μm in size (less than 20%). The regions shown in the images represent the former. There is no difference in the amount and distribution of the secondary phase between the slip cast and dry pressed samples.

Typical EDX spectra from the samples are shown in Fig. 5. The carbon peak in Fig. 5a is due to the thin conducting C layer deposited on all the TEM samples. The matrix grains in all the samples contain only Al and O, indicating pure alumina. Slight variations were observed in the compositions of the boundary phases in the different samples. In the 98% samples, SC98-2 (Fig. 2a) and DP98-1 (Fig. 2c) show a small amount of a secondary phase containing Ca and Si, whereas, the secondary phases are more prevalent in SC98-1 and DP98-2 (Fig. 2b and d) and they contain substantial amounts of Si and Ca. In the 95% and 91% samples, some areas also contain Mg, in trace quantities, in addition to Si and Ca (Fig. 5d). The Mg-rich phase is more pronounced in the 95% samples and was detected in both the SEM-EDX and TEM-EDX analyses, whereas, the SEM-EDX analysis did not show the presence of Mg in the 91% samples.

Generally, the samples contain two main types of secondary phases. The compositions inferred from the spectra with the assumption of a thin film limit are roughly 73% SiO_2, 15% Al_2O_3, and 12% CaO by weight for one (Fig. 5b) and 42% SiO_2, 35% Al_2O_3, and 23% CaO for the other (Fig. 5c). One phase is predominantly SiO_2 while the other contains Al_2O_3 and CaO in more substantial quantities. Analysis of the diffraction patterns shows the alumina matrix to be α-Al_2O_3, i.e., corundum (Fig. 6a). The secondary phase, with high alumina content, is crystalline (Fig. 6b) and identified as anorthite, and the SiO_2-rich phase is amorphous (diffuse ring in Fig. 6c). The spots in Fig. 6c are from the matrix phase. No diffraction pattern was obtained for the Mg-rich phase because the areas where it was found were too small. However, with the XRD analysis, the phase was identified as spinel

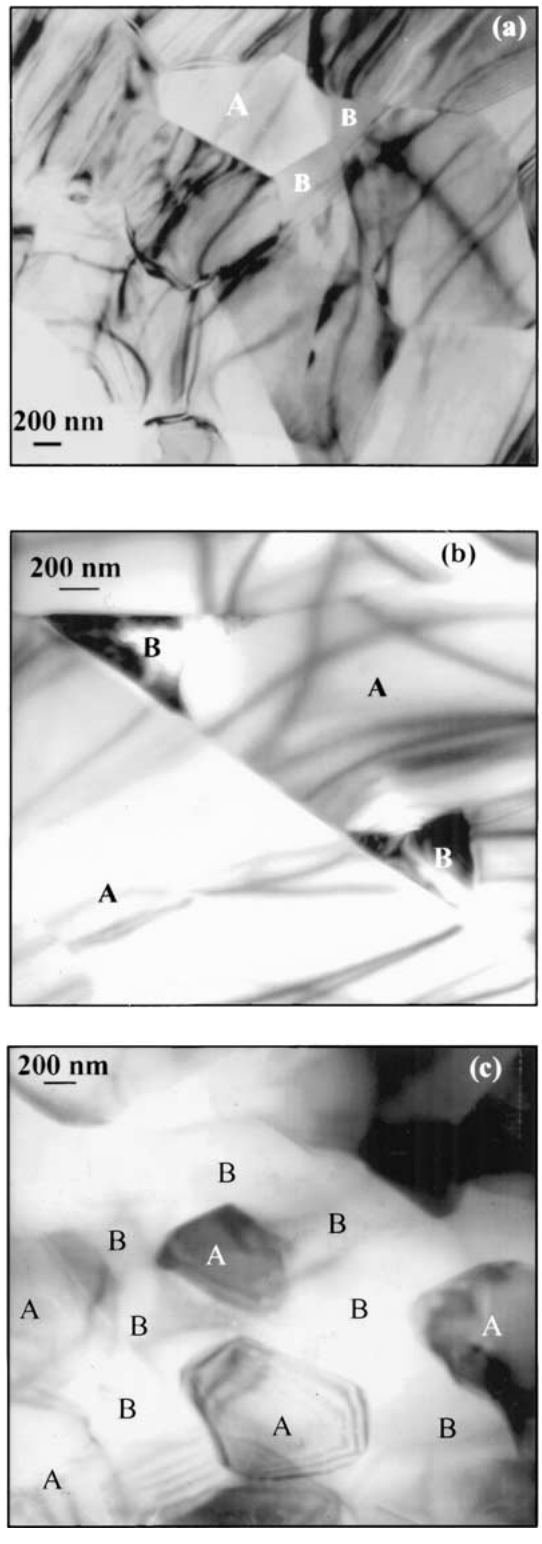

Figure 4 Typical TEM images of the ceramic samples. (a) 98% alumina; (b) 95% alumina; (c) 91% alumina. A denotes alumina grains and B denotes boundary phases.

($MgAl_2O_4$) in the two 95% alumina samples (Fig. 7). No additional phase (other than corundum and anorthite) was identified in the 91% alumina samples, despite the relatively high percentage of additives. This may be an indication that any additional phases may be amorphous and/or below the dectectability limit of XRD. Powell-Dogan and Heuer [15, 18] have shown that the phases in high alumina ceramics depend on

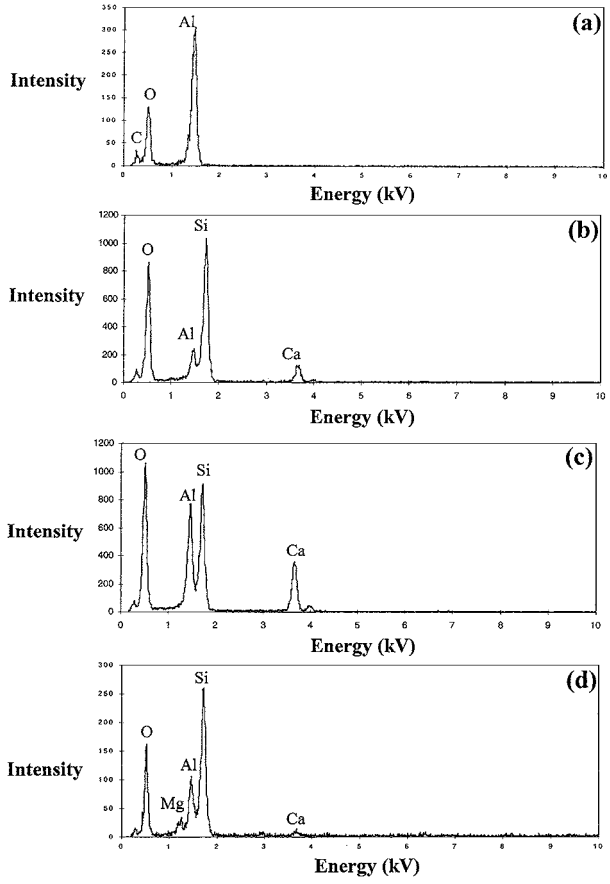

Figure 5 Typical TEM EDX spectra from the ceramic samples. (a) Matrix alumina grains; (b) amorphous boundary phase; (c) crystalline boundary phase (anorthite); (d) Mg-containing boundary phase in 95% and 91% samples.

the initial boundary glass composition and the thermal history.

4. General discussion

The trends in the mechanical behaviour of ceramics, as reported by Lawn *et al*. [21] and Cook *et al*. [22], show a characteristic transition from indentation-controlled behaviour to microstructure-controlled behaviour as a function of the ratio of crack size to grain size. In particular, strength trends for ceramics with microstructures of different characteristic dimension appear to be consistent with a systematic increase in material toughness as the ratio of crack size to grain size increases [23–28]. This toughening effect may reflect an intrinsic change from single-crystal to polycrystalline behaviour as the crack grows from subgrain to multigrain dimensions [23, 24, 26]. Lawn *et al*. [21] and Cook *et al*. [22] have used the indentation technique to investigate the microscopic-to-macroscopic crack-size transition in coarse-grained alumina ceramics and their plots of normalized apparent toughness as function of indentation loads are reproduced in Fig. 8. Indentation flaws were introduced into the strength specimens and the size of the cracks varied systematically with the contact load. In direct analogy to the R-curve effects reported in other crack propagation configurations, at the lower end of the crack-size spectrum the toughness is determined by single-crystal cleavage energies (transgranular fracture) or grain-boundary energies (intergranular fracture). At large crack sizes the microstructural influence is "averaged out," and the toughness becomes representative of the polycrystalline aggregate [22]. As shown in Fig. 8a, the transition indentation load varies for different materials and different grain structure [21]. The P/N in Fig. 8a represents indentation load P in Newtons (N) and D is the grain size. The normalized values in Fig. 8b were obtained by dividing the apparent toughness, K_c^{app}, where K_c^{app} levels out, by the polycrystalline toughness, K_c^{∞}, and the indentation load P by the characteristic transition load, P^*, for the different samples.

TABLE IV Hardness and fracture toughness at different indentation loads

Load→ Sample ↓	100 N		200 N	
	H_v (Kg/mm^2)	K_c (MPa · m$^{1/2}$)	H_v (Kg/mm^2)	K_c (MPa · m$^{1/2}$)
SC98-1	1288 ± 37	3.09 ± 0.25	1314 ± 49	2.63 ± 0.22
SC98-2	1354 ± 34	2.98 ± 0.12	1254 ± 179	2.88 ± 0.59
DP98-1	1402 ± 75	2.91 ± 0.41	1239 ± 253	3.30 ± 1.02
DP98-2	1478 ± 44	2.77 ± 0.19	1283 ± 74	2.97 ± 0.37
SC95-1	1097 ± 58	2.33 ± 0.30	965 ± 154	2.05 ± 0.62
SC95-2	1187 ± 66	2.30 ± 0.27	1171 ± 51	2.41 ± 0.21
SC91-1	1132 ± 35	2.51 ± 0.11	1049 ± 100	2.46 ± 0.38
SC91-2	1150 ± 16	2.37 ± 0.22	1145 ± 33	2.31 ± 0.21
DP91-1	1168 ± 34	2.37 ± 0.23	1158 ± 42	2.43 ± 0.29

To compare mechanical properties of materials, it must be shown that the property is in the same region on the R-curve for the different samples. Except for SC98-1, within the limits of experimental errors, the results for 100 N and 200 N compared in Table IV appear not to be significantly different, indicating that the values lie within the polycrystalline toughness plateau region. The SC98-1 behaviour falls into the single-crystal toughness region and this is consistent with the relatively coarse grain structure of the sample (Fig. 2b). In addition to correlating processing and microstructures of the samples, attempt is also made to explain the properties in terms of the microstructures.

4.1. Grain structure and properties

The grain structure and properties of the samples are not significantly affected by the manufacturing method (Figs 2 and 3 and Table II). The dry pressed samples have a slightly finer grain structure and exhibit slightly higher hardness, lower fracture toughness and are slightly more brittle. Generally, fracture toughness decreases and index of brittleness increases with increasing hardness. Grain size appears to decrease and the distribution is more uniform, with decreasing alumina content.

The MgO content of the additives in the 98% alumina samples is relatively low and this could be the reason for the wide distribution of grain sizes and the isolated pores trapped within larger grains (Fig. 2). In addition to helping to reduce sintering temperature and time, MgO is known to prevent discontinuous grain growth and

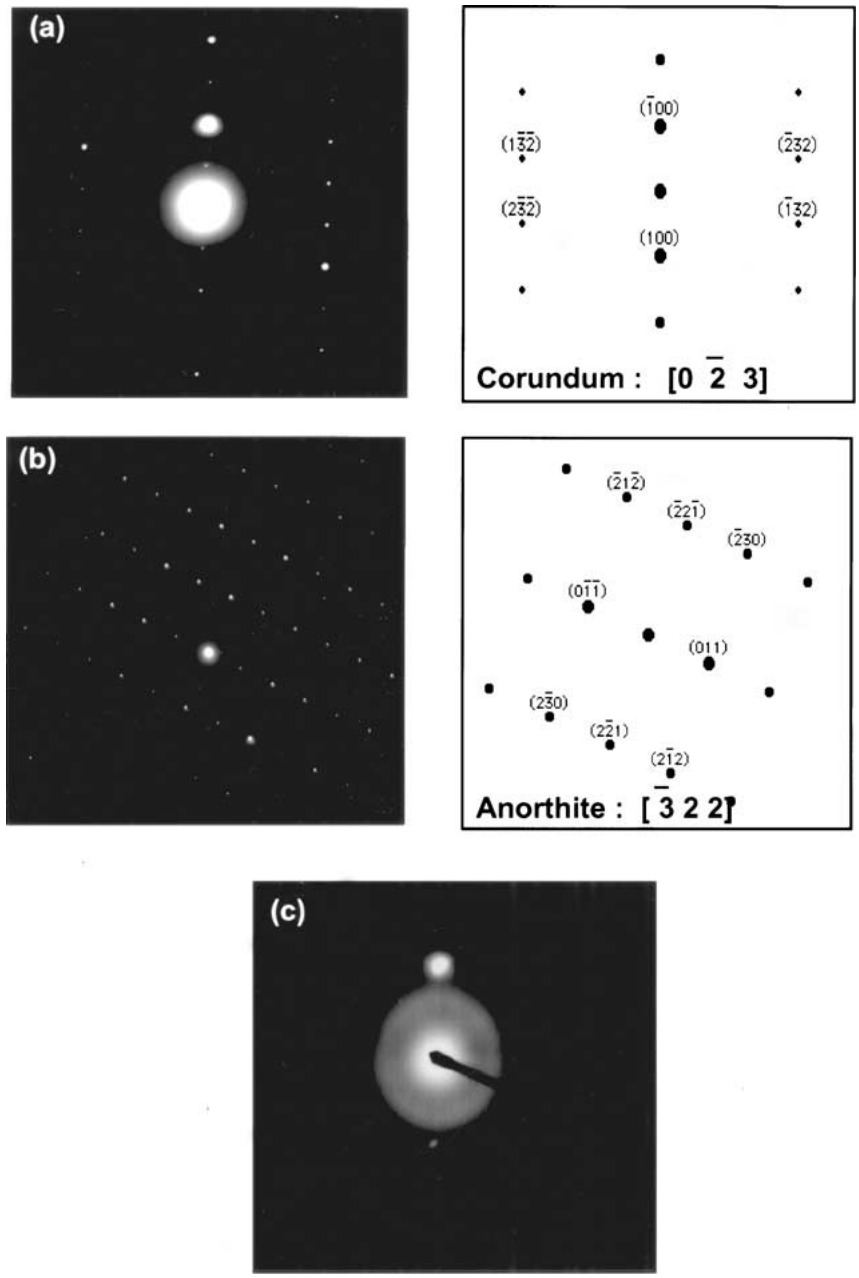

Figure 6 Typical diffraction patterns from (a) alumina matrix, and (b, c) intergranular secondary phases.

allows sintering to theoretical or near theoretical density [29–31]. Discontinuous grain growth means that grain boundaries break away from the pores, thereby including the pores in the new large grains. The obvious effect of discontinuous grain growth is lower strength. The SiO_2 content is responsible for the predominant silicate glassy phase, a weak link between the grains of the alumina matrix [17]. Both undoped and $CaSiO_3$-doped materials have been reported to be susceptible to exaggerated growth of a small fraction of the grains in the sample, leading to wide distributions of grain sizes and frequently to isolated pores trapped within the larger grains [32].

The presence of CaO impurities has less influence on sintering; they have, however, a long-term effect in reducing the mechanical strength of alumina ceramics [33, 34], due to calcium migration and segregation and reaction with the environment [35–37]. The relative proportions of the SiO_2, CaO and MgO in the additives, therefore, play a principal role in sintered alumina microstructure and properties.

4.2. Secondary phases

All the samples are shown to contain, as secondary phases, anorthite and a glassy phase with varying proportions of Al_2O_3, SiO_2, and CaO. $CaSiO_3$-doped alumina has been shown to contain a glassy grain-boundary phase, said to be indicative of liquid-phase sintering [32, 38], but the presence of anorthite has not been widely reported.

The Mg-containing secondary phase found in some of the samples is consistent with what is reported in literature. The microstructures of alumina doped with

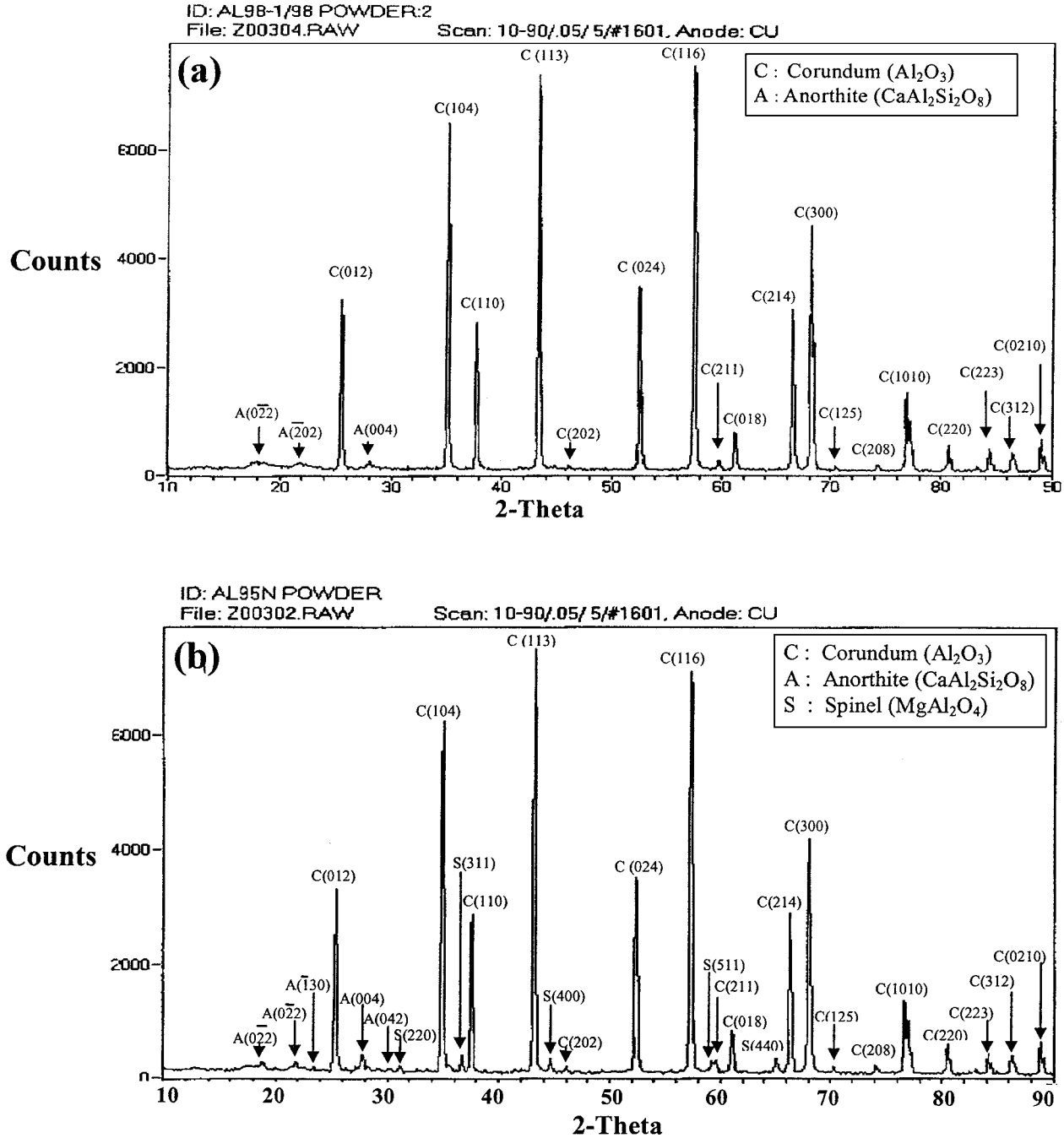

Figure 7 Typical spectra from the X-ray powder diffractometry analysis. (a) Most samples except 95% alumina samples; (b) 95% samples showing an additional phase, spinel.

0.2–0.5 wt% MgO have been reported to contain spinel, $MgAl_2O_4$ [29, 39]. XRD analysis of a commercial 85 wt% Al_2O_3 by Travitzky *et al.* [40] shows the presence of corundum, spinel and small amounts of anorthite and cordierite ($2MgO \cdot 2Al_2O_3 \cdot 5SiO_2$). The solubility of Mg in Al_2O_3 is very limited. Roy and Coble [41] measured the Mg solubility in the range of the usual sintering temperatures and reported 1400 ppm at 1830°C and 300 ppm at 1630°C. The maximum solubility of Mg in Al_2O_3 is approximately 1 wt% at 1975°C [42]. Spinel is formed when the MgO content exceeds the solubility limit and even for levels below and up to the solubility limit, segregation of Mg at the grain boundaries has been reported [43]. The presence of spinel has also been observed in other high Al_2O_3-ceramics [18, 44]. The MgO content in the 98% alumina samples is very small and well below the solubility limit, hence, no trace of Mg is shown in any of the chemical analyses. XRD analysis indicates the presence of spinel in the 95% alumina samples but not in the 91% samples, although the TEM energy dispersive x-ray analysis does indicate the presence of Mg in some of the secondary phases. The MgO content of the additives in the 95% and 91% alumina samples is the same and the only difference is the SiO_2 content, which is higher for the 91% samples. The higher SiO_2 content may have suppressed the formation of spinel or reduced it to below the detection level in the XRD analysis. It is also possible that the Mg-containing secondary phase in the 91% sample is amorphous.

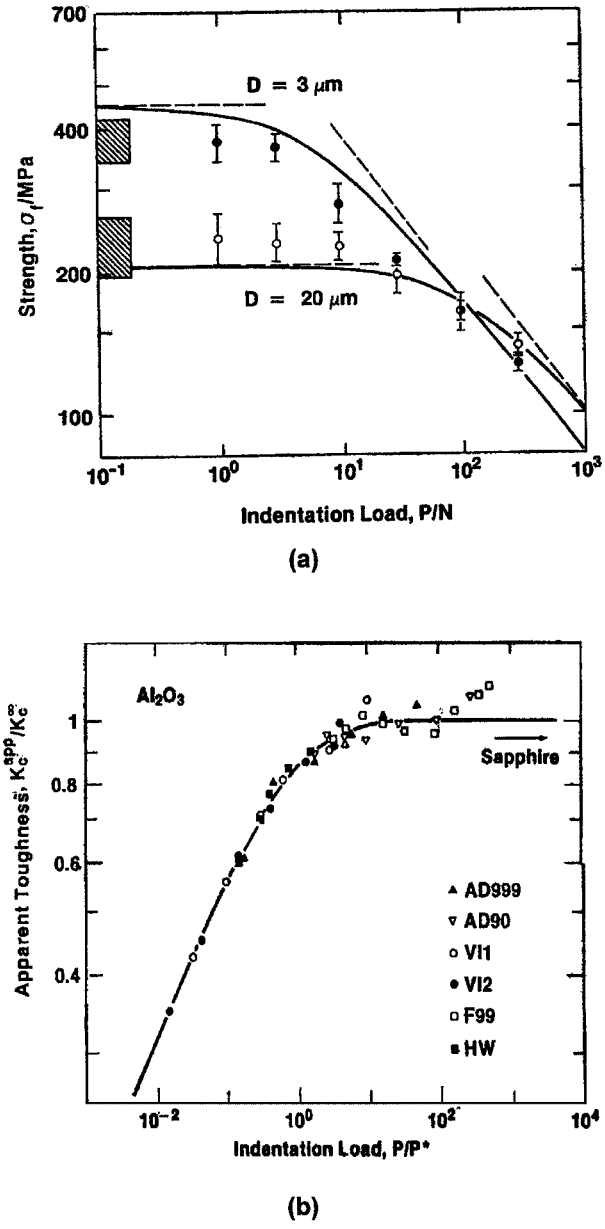

Figure 8 (a) Strength characteristics of alumina ceramics with two grain sizes [21]. (b) Normalized apparent toughness of alumina ceramics [22] as a function of indentation loads.

5. Conclusions

The various alumina ceramic samples have been investigated for their hardness, fracture toughness and microstructural characteristics and the following conclusions are drawn:

1. An indentation technique has been applied and shown to work reasonably well for the determination of the fracture toughness of all the ceramic samples. A load of 100 N was determined to be optimal for this technique.

2. The expression used for the determination of the relative index of brittleness provides a reasonable pattern, which is consistent with established fact.

3. Generally, for a given alumina content the fracture toughness decreases with increasing hardness.

4. The fracture toughness and hardness values are higher for the 98% alumina samples but the differences between the lower alumina samples are negligible.

5. The hardness values of the dry pressed samples appear to be slightly higher than for the slip cast samples, although, their fracture toughness values are lower.

6. Significant effects of the processing parameters in slip casting are demonstrated, with the SC98-2 showing a superior microstructure with a finer grain structure and better mechanical properties than the SC98-1. SC98-2 was manufactured using an optimized process.

7. The effects of slip properties and spray drying parameters in dry pressing are demonstrated with different microsrostructures and properties shown for DP98-1 and DP98-2. The grain structure is a bit finer for DP98-2 and it shows a slightly higher hardness, lower fracture toughness and slightly higher index of brittleness.

8. The grain sizes of the samples are bimodal with the majority ≤ 3 μm in size. The size range narrows with decreasing alumina content. The wide grain size distribution in the 98% alumina samples may be due to the low MgO content of the additives.

9. The microstructures of the ceramic samples are composed of a matrix phase, corundum (α-Al_2O_3), and grain boundary phases which consist of a glassy phase with varying Al, Si and Ca contents and a crystalline phase, triclinic anorthite ($CaAl_2Si_2O_8$). Mg-rich phases were found in the 95% and 91% alumina samples. The phase was identified by XRD as spinel in the 95% samples.

Acknowledgements

The authors are grateful to the University of Alberta Advanced and Engineered Materials (UAAEM) Centre and Ceramic Protection Corporation (CPC), Calgary for providing the funding and samples (CPC) for this work.

References

1. E. DORRE and H. HUBNER, "Alumina: Processing, Properties and Applications," Materials Research and Engineering (Springler-Verlag, Berlin, Germany, 1984).
2. Ceramic Protection Corporation, (CPC), Calgary, Development of spray drying process for high alumina ceramics tile pressing, internal communication, 1997.
3. W. D. KINGERLY, "Ceramic Fabrication Processes," (The Technology Press of Massachusetts Institute of Technology, 1958) p. 57.
4. P. OSTOJIC and R. MCPHERSON, *Int. J. Fract.* **33** (1987) 297.
5. R. W. HERTZBERG, "Deformation and Fracture Mechanics of Engineering Materials," 3rd ed. (John Wiley & Sons, Toronto, 1989) p. 303.
6. D. B. MARSHALL, T. NOMA and A. G. EVANS, *Comm. Am. Ceram. Soc.* **65** (1982) C-175.
7. B. R. LAWN and V. R. HOWES, *J. Mater. Sci.* **16** (1981) 2745.
8. B. R. LAWN and D. B. MARSHALL, *J. Amer. Ceram. Soc.* **62** (1979) 347.
9. B. J. DALGLEISH, P. L. PRATT and J. SANDFORD, *Sci. Mater.* **8** (1976) 225.
10. L. A. SIMPSON, *J. Amer. Ceram. Soc.* **56** (1973) 7.
11. P. L. GUTSHALL and D. E. GROSS, *Eng. Fract. Mech.* **1** (1969) 463.
12. G. D. SWANSON, *J. Amer. Ceram. Soc.* **55** (1972) 48.
13. P. L. PRATT, Mechanics and Physics of Fracture, Institute of Physics, 1975, paper 22.
14. R. STEINBRECH, R. KHEHANS and W. SCHAARWACHTER, *J. Mater. Sci.* **18** (1983) 265.
15. C. A. POWELL-DOGAN and A. H. HEUER, *J. Amer. Ceram. Soc.* **74** (1991) 646.

16. T. H. COURTNEY, "Mechanical Behaviour of Materials," (McGraw-Hill Publishing Company, New York, 1990) p. 483.
17. E. DORRE and H. HUBNER, "Alumina: Properties, Processing and Applications," Materials Research and Engineering (Springer-Verlag, Berlin, Germany, 1984).
18. C. A. POWELL-DOGAN and A. H. HEUER, *J. Amer. Ceram. Soc.* **73** (1990) 3670.
19. S. C. HANSEN and D. S. PHILLIPS, *Philos. Mag. A.* **47** (1983) 209.
20. Y. K. SIMPSON and C. B. CARTER, in Proc. 46th Electron Microscopy Society of America Meetings, San Francisco, CA (1988) p. 570.
21. B. R. LAWN, S. W. FREIMAN, T. L. BAKER, D. D. COBB and A. C. GONZALEZ, *J. Amer. Ceram. Soc.* **67**(4) (1984) C-67.
22. R. F. COOK, B. R. LAWN and C. J. FAIRBANKS, *ibid.* **68**(11) (1985) 604.
23. S. M. WIEDERHORN, in "Mechanical and Thermal Properties of Ceramics," edited by J. B. Wachtman, Jr., Natl. Bur. Stand. (U.S.) Spec. Publ., no. 303, (1969) 217.
24. R. W. RICE, in "Fracture Mechanics of Ceramics," Vol. 1., edited by R. C. Bradt, D. P. H. Hasselman and F. F. Lange (Plenum, New York, 1974) p. 323.
25. R. W. RICE, S. W. FREIMAN and J. J. MECHOLSKY, *J. Amer. Ceram. Soc.* **63**(3/4) (1980) 129.
26. J. P. SINGH, A. V. VIRKAR, D. K. SHETTY and R. S. GORDON, *ibid.* **62**(3/4) (1979) 179.
27. A. G. EVANS, *ibid.* **63**(1/2) (1980) 703.
28. A. V. VIRKAR, D. K. SHETTY and A. G. EVANS, *ibid.* **64**(3) (1981) C-56.
29. G. ROSSI and J. W. BURKE, *ibid.* **56** (1973) 654.
30. R. L. COBLE, *J. Appl. Phys.* **32** (1961) 793.
31. H. P. CAHOON and C. J. CHRISTENSEN, *J. Amer. Ceram. Soc.* **39** (1956) 337.
32. S. C. HANSEN and D. S. PHILLIPS, *Philos. Mag.* **47** (1961) 209.
33. A. W. FUNKENBUSCH and D. W. SMITH, *Met. Trans. A* **6** (1975) 2299.
34. S. SUNHAVOY, L. L. LAVENSON, W. V. PALLAND and D. E. S. DAY, *Amer. Ceram. Soc. Bull.* **57** (1978) 231.
35. H. L. MARCUS and M. E. FINE, *J. Amer. Ceram. Soc.* **55** (1972) 568.
36. W. C. JOHNSON and D. F. STAIN, *ibid.* **58** (1975) 485.
37. D. R. CLARKE, *ibid.* **63** (1980) 339.
38. D. S. PHILLIPS and Y. R. SHIUE, *Adv. Ceram.* **10** (1984) 357.
39. C. LI and W. D. KINGERY, *ibid.* **10** (1984) 368.
40. N. A. TRAVITZKY, D. G. BRANDON and E. Y. GUTMANAS, *Mater. Sci. Eng. A* **71** (1985) 77.
41. S. K. ROY and R. L. COBLE, *J. Amer. Ceram. Soc.* **51** (1968) 1.
42. D. VIECHNICKI, F. SCHMID and J. W. MCCAULEY, *ibid.* **57** (1974) 47.
43. F. E. C. FRANKEN and A. P. GEHRING, *J. Mater. Sci.* **16** (1981) 384.
44. S. M. WIEDERHORN, B. J. HOCKEY, R. F. KRAUSE and K. JAKUS, *ibid.* **21** (1986) 810.

Received 6 June 2000
and accepted 31 May 2001